Evolution of anisotropic turbulence in nonlinear magnetic reconnection

M. Onofri* and F. Malara
Dipartimento di Fisica, Università della Calabria, via P. Bucci, 87036 Rende (CS), Italy
(Received 13 December 2007; published 11 July 2008)

The anisotropy properties of magnetohydrodynamic turbulence in a sheared magnetic field are analyzed through a three-dimensional numerical simulation that reproduces the linear and nonlinear stage of a tearing instability. Far from the current sheet, the energy spectrum develops perpendicularly to the local magnetic field, as in homogeneous configurations. Within the current sheet, the spectrum anisotropy is also affected by the structure of unstable modes. With increasing time, the configuration becomes more turbulent, the former effect disappears, and the energy cascade takes place perpendicularly to the local magnetic field. The local spectrum becomes increasingly anisotropic while the spatially integrated spectrum tends to isotropize. There is the possibility that these properties could be used to identify the nonlinear stage of magnetic reconnection in space and laboratory plasmas, as well as to identify the particle transport regime in the considered magnetic configuration.

DOI: 10.1103/PhysRevE.78.016402 PACS number(s): 52.35.Ra, 52.35.Vd

I. INTRODUCTION

The properties of magnetohydrodynamic (MHD) turbulence are affected by the presence of a large-scale background magnetic field, which produces spectral anisotropy [1]. Evidence of anisotropy in MHD turbulence has been found in the solar wind [2], in various regions of the Earth's magnetosphere [3], and in laboratory plasmas [4]. The effect of a background magnetic field on the development of MHD turbulence has also been investigated in more complex configurations, such as a current sheet subject to tearing instability [5]: when reconnecting unstable modes grow to significant amplitudes, they interact nonlinearly producing an energy cascade to small scales. Magnetic reconnection has been recognized in the turbulent magnetosheath through the observation of electric and magnetic fields [6,7]. Evidence of magnetic reconnection in the solar wind has been found in observations of plasma jets emanating from reconnection sites [8–11]. In the present paper, we analyze some specific characteristics of the turbulence anisotropy produced in a tearing-unstable current sheet. The resulting fluctuation spectrum has a complex pattern in the wave-vector space, with a peculiar variation both with the position within the current sheet and in time. Such properties may be useful to identify reconnection events in space plasmas or in laboratory devices. The presence of anisotropic fluctuations in MHD turbulence can also affect the transport of energetic particles in a mean magnetic field, where the transport regime depends on the turbulence anisotropy [12,13].

The anisotropy observed in MHD turbulence is due to a larger rate of energy transfer in the direction perpendicular to the large-scale magnetic field. Using the Elsässer variables $\mathbf{z}^{\pm}=\mathbf{V}_1 \pm \mathbf{B}_1$ [14], the ideal incompressible MHD equations in dimensionless units are written

$$\frac{\partial \mathbf{z}^{\pm}}{\partial t} \mp \mathbf{v}_A \cdot \nabla \mathbf{z}^{\pm} + \mathbf{z}^{\mp} \cdot \nabla \mathbf{z}^{\pm} = -\nabla p \tag{1}$$

with $\nabla \cdot \mathbf{z}^{\pm}=0$, where $\mathbf{V}_1$ and $\mathbf{B}_1$ are the velocity and magnetic-field fluctuations, p is the total (kinetic+magnetic) pressure, and $\mathbf{v}_A$ is the Alfvén velocity directed along the background magnetic field $\mathbf{B}_0$. Equation (1) indicates that the small-scale turbulence can be considered as formed by Alfvènic perturbations, with nonlinear interactions occurring only between modes traveling in opposite directions (term $\mathbf{z}^{\mp} \cdot \nabla \mathbf{z}^{\pm}$). The term $\mathbf{v}_A \cdot \nabla \mathbf{z}^{\pm}$ describes the propagation of perturbations along $\mathbf{B}_0$, which weakens the interactions between perturbations. For two counterpropagating perturbations with wave vectors $\mathbf{k}_1$ and $\mathbf{k}_2$, the interaction time is $\tau_I \sim \max\{(\mathbf{k}_1 \cdot \mathbf{v}_A)^{-1}, (\mathbf{k}_2 \cdot \mathbf{v}_A)^{-1}\}$. Therefore, nonlinear interactions between waves with $\mathbf{k}$ quasiperpendicular to $\mathbf{B}_0$ are more efficient than when $\mathbf{k}$ is nearly parallel to $\mathbf{B}_0$. Thus, the energy cascade takes place mainly in the direction perpendicular to the mean magnetic field.

This kind of anisotropy has been usually studied in configurations with a uniform $\mathbf{B}_0$. The original two-dimensional studies of Shebalin *et al.* [1] were extended to three dimensions by Oughton *et al.* [15], who investigated the development of anisotropy from initially isotropic conditions. They found that in the presence of a uniform magnetic field $\mathbf{B}_0$, energy is transferred preferentially to modes with wave numbers perpendicular to $\mathbf{B}_0$. Anisotropy has also been studied relative to the direction of the local mean magnetic field in configurations with or without a uniform background magnetic field [16,17]. In these studies, the anisotropy direction varies with space. Some of the results obtained in the present study are consistent with the results in Refs. [16,17]. The configuration studied in the present work is different for two reasons: (i) the presence of a large-scale current sheet, with a sheared equilibrium magnetic field; (ii) the energy cascade is also affected by the spatial pattern of tearing-unstable modes that initiate the cascade.

II. THE MODEL

We solve numerically the MHD equations (1) written in the form

*onofri@fis.unical.it

$$\frac{\partial \mathbf{V}}{\partial t} + (\mathbf{V}\cdot\nabla)\mathbf{V} = -\nabla p + (\mathbf{B}\cdot\nabla)\mathbf{B} + \frac{1}{R_v}\nabla^2\mathbf{V}, \tag{2}$$

$$\frac{\partial \mathbf{B}}{\partial t} = \nabla \times \left(\mathbf{V}\times\mathbf{B} + \frac{1}{R_M}\nabla\times\mathbf{B}\right), \tag{3}$$

$$\nabla^2 p = \nabla\cdot[(\mathbf{B}\cdot\nabla)\mathbf{B} - (\mathbf{V}\cdot\nabla)\mathbf{V}], \tag{4}$$

where dissipative terms have been added to Eqs. (2) and (3), R_v and R_M being the kinetic and magnetic Reynolds numbers. The three-dimensional spatial domain is $D=[-1,+1]\times[0,2\pi]\times[0,2\pi]$. Periodic boundary conditions are imposed in the y and z directions while boundary conditions at $x=\pm 1$ correspond to perfectly conducting walls,

$$B_x|_{x=\pm 1} = \mathbf{V}|_{x=\pm 1} = 0, \tag{5}$$

$$\left.\frac{dB_y}{dx}\right|_{x=\pm 1} = \left.\frac{dB_z}{dx}\right|_{x=\pm 1} = \left.\frac{dp}{dx}\right|_{x=\pm 1} = 0. \tag{6}$$

We choose as unit measure for the magnetic field a typical value B_0, which allows us to define a characteristic value of the Alfvén velocity $v_A=B_0/\sqrt{4\pi\rho}$. The quantity ρ is the mass density, uniform everywhere. Hence, we express the velocity in terms of v_A and the time in terms of the typical Alfvén time: $\tau_A=L_x/v_A$. Finally, the pressure P is measured in units of ρv_A^2, while the definition of the Reynolds numbers, in terms of the kinematic viscosity ν and of the resistivity η, is $R_v=v_A L_x/\nu$ and $R_M=v_A L_x/\eta$.

The background configuration is given by a vanishing velocity $\mathbf{V}_0=\mathbf{0}$ and a magnetic field $\mathbf{B}_0$ sheared along the x direction, with a current sheet in the middle of the simulation domain: $\mathbf{B}_0=B_{y0}\hat{y}+B_{z0}(x)\hat{z}$, where $B_{y0}=0.5$ is a constant value, while B_{z0} is given by

$$B_{z0}(x) = \tanh\left(\frac{x}{a}\right) - \frac{x/a}{\cosh^2(1/a)}. \tag{7}$$

This form for the magnetic field [in particular the last term in Eq. (7)] ensures that the first derivatives along $\hat{x}$ of all the components of the magnetic field vanish at the boundaries, to be consistent with the boundary conditions. The parameter $a=0.1$ represents the width of the current sheet and it has been chosen small enough to reduce stabilizing effects from the walls. The background total pressure p_0 is computed by solving Eq. (4).

III. LINEAR THEORY

It is useful to study the behavior of perturbations in the limit of small amplitude. This should describe what happens in the first stage of the time evolution and it will be useful to understand the results of the numerical simulation described in Sec. IV, based on the fully nonlinear equations (2)–(4). Assuming that $\mathbf{B}_0$, $\mathbf{V}_0$, and P_0 represent an equilibrium with $\mathbf{V}_0=\mathbf{0}$ and $\mathbf{B}_0=B_{0y}(x)\hat{y}+B_{0z}(x)\hat{z}$, which is perturbed with an infinitesimal perturbation of amplitude $\varepsilon \ll 1$, the magnetic field, velocity, and pressure can be decomposed as follows:

$$\mathbf{B} = \mathbf{B}_0 + \varepsilon\mathbf{B}_1, \tag{8}$$

$$\mathbf{V} = \mathbf{V}_0 + \varepsilon\mathbf{V}_1, \tag{9}$$

$$P = P_0 + \varepsilon P_1. \tag{10}$$

Substituting the above quantities in the MHD equations (2) and (3), and neglecting the nonlinear terms, proportional to ε^2, we obtain the linearized MHD equations,

$$\frac{\partial \mathbf{V}_1}{\partial t} = -\nabla P_1 + (\nabla\times\mathbf{B}_0)\times\mathbf{B}_1 + (\nabla\times\mathbf{B}_1)\times\mathbf{B}_0 + \frac{1}{R_v}\nabla^2\mathbf{V}_1, \tag{11}$$

$$\frac{\partial \mathbf{B}_1}{\partial t} = \nabla\times(\mathbf{V}_1\times\mathbf{B}_0) + \frac{1}{R_M}\nabla^2\mathbf{B}_1. \tag{12}$$

Taking the curl of Eq. (11), the pressure is eliminated and we look for solutions in the form

$$\mathbf{B}_1(x,y,z,t) = \tilde{\mathbf{B}}_1(x)e^{i(k_y y+k_z z)}e^{\gamma t}, \tag{13}$$

$$\mathbf{V}_1(x,y,z,t) = \tilde{\mathbf{V}}_1(x)e^{i(k_y y+k_z z)}e^{\gamma t}. \tag{14}$$

Magnetic reconnection takes place on resonant surfaces defined by the condition $\mathbf{k}\cdot\mathbf{B}_0=0$. The positions of the resonant surfaces are determined by the ratio k_y/k_z. The growth rate γ and the spatial dependence $\tilde{\mathbf{B}}_1(x)$, $\tilde{\mathbf{V}}_1(x)$ of the corresponding eigenmodes are calculated by a numerical procedure. It is useful to rotate the reference frame and to write the perturbations of magnetic field and velocity in the following form:

$$\mathbf{B}_1 = \nabla\times(\Psi\hat{\mathbf{e}}_3) + b\hat{\mathbf{e}}_3, \tag{15}$$

$$\mathbf{V}_1 = \nabla\times(\Phi\hat{\mathbf{e}}_3) + v\hat{\mathbf{e}}_3, \tag{16}$$

where the unity vector $\hat{\mathbf{e}}_3$ is defined as $\hat{\mathbf{e}}_3=\hat{x}\times\mathbf{k}/k$. Using these expressions in the linearized equations, we obtain two ordinary differential equations for the two potentials Ψ and Φ:

$$\gamma\Psi = kF\Phi + \frac{1}{R_M}\left(\frac{d^2\Psi}{dx^2} - k^2\Psi\right),$$

$$\gamma\left(\frac{d^2\Phi}{dx^2}\right) = \Psi k\frac{d^2F}{dx^2} + kF\left(k^2\Psi - \frac{d^2\Psi}{dx^2}\right) + \frac{1}{R_v}\left(2k^2\frac{d^2\Phi}{dx^2} - \frac{d^4\Phi}{dx^4} - k^4\Phi\right),$$

where the function F is defined as $F(x)=\mathbf{B}_0(x)\cdot\mathbf{k}$. These equations can be transformed into six first-order differential equations for the variables Ψ, Φ, $d\Psi/dx$, $d\Phi/dx$, $d^2\Phi/dx^2$, and $d^3\Phi/dx^3$. We wrote a code to solve these linearized equations (linear code). This code solves a system of N first-order ordinary differential equations with N boundary conditions, but in our case the number of unknowns is larger than the number of equations because the linearized MHD equations depend on the growth rate γ, so a system of six equations and seven unknown quantities must be solved. If seven conditions are imposed on the boundaries, a solution exists only for a particular value of γ and it can be found treating γ

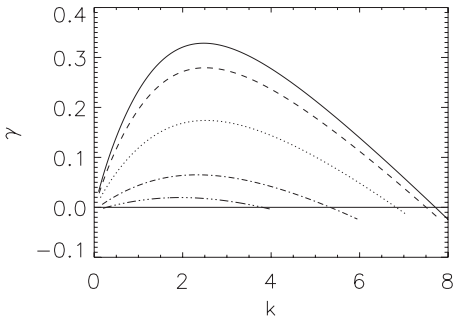

FIG. 1. Growth rates of unstable modes for $R_M=10^3$, $R_v=10^3$, and different values of the ratio k_y/k_z: $k_y/k_z=0$ (solid line), $k_y/k_z=0.5$ (dashed line), $k_y/k_z=1$ (dotted line), $k_y/k_z=1.5$ (dot-dashed line), and $k_y/k_z=1.75$ (triple-dot-dashed line).

as another variable and introducing another equation,

$$\frac{d\gamma}{dx}=0,$$

which imposes that γ is a constant. One of the boundary conditions can be used to fix the amplitude of the eigenmodes, which is arbitrary, while the remaining six conditions impose vanishing values for Ψ, Φ, and $d\Phi/dx$ at the two boundaries. These conditions derive from those imposed in the simulation for B_x and $\mathbf{V}$, Eqs. (5) and (6). The numerical method employed by the linear code is based on a relaxation technique. Starting from an initial guess for the solution $\mathbf{S}$, the corrections $\delta\mathbf{S}$ are determined so that $\mathbf{S}+\delta\mathbf{S}$ is a better approximation of the solution. This procedure is repeated until the corrections become sufficiently small. In Fig. 1, the growth rates γ calculated from the linearized equations are plotted as a function of the modulus of the wave vector for different values of the ratio k_y/k_z. The growth rate is maximum for $k_y=0$. This corresponds to a resonant surface located in the center of the current sheet ($x=0$). The growth rate decreases with increasing the ratio k_y/k_z, i.e., when the resonant surface is increasingly off the center of the current sheet. An example of the eigenmodes is shown in Fig.2 for a case with $k_y=0$ and $k_z=2$.

IV. NONLINEAR EVOLUTION

We solved the nonlinear MHD equations (2)–(4), with the boundary conditions specified in Sec. II, by means of a numerical simulation. The initial condition is obtained by superposing three-dimensional divergenceless fluctuations with amplitude $\epsilon=10^{-4}$ (satisfying the boundary conditions) to the background fields (7).

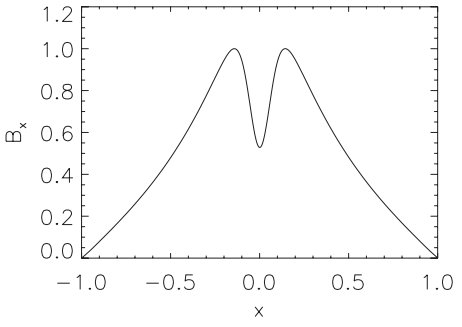

FIG. 2. The x component of magnetic-field perturbation in a linear unstable mode with $R_M=10^3$, $R_v=10^3$, $k_y=0$, and $k_z=2$.

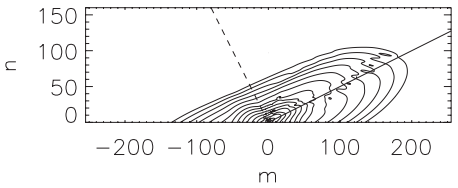

FIG. 3. Contour plots of the total energy spectrum $\log_{10}[E^{\mathrm{tot}}_{m,n}(x,t)]$ at $t=35$ and $x=-0.5$. The dashed line indicates the local direction of $\mathbf{B}_0$ and it is perpendicular to the solid line.

To solve Eqs. (2)–(4), we used a compact finite-difference scheme in the inhomogeneous direction (x) and a pseudospectral method in the periodic directions (y and z). For details on the numerical method, see Ref. [18]. Each quantity $f(x,y,z,t)$ is expanded in Fourier series, according to

$$f(x,y,z,t)=\sum_{m=-N_y/2}^{N_y/2}\sum_{n=0}^{N_z} f_{m,n}(x,t)e^{[i(my+nz)]}, \tag{17}$$

where m and n are the (integer) wave numbers in the y and z directions, respectively. At the initial time, the background magnetic field $\mathbf{B}_0$ corresponds to the Fourier harmonic $\mathbf{B}_{0,0}(x,0)$. During the subsequent evolution, we keep this harmonic constant to avoid magnetic diffusion; thus, the width of the current sheet does not increase in time. We used the values

$$N_x=128,\quad N_y=512,\quad N_z=1024,$$

$$R_v=1000,\quad R_M=1000.$$

The equilibrium has been perturbed by exciting Fourier harmonics with $-4\le m\le 4$ and $0\le n\le 4$.

The time evolution shows an exponential growth of several unstable modes [5]. When their amplitudes become large enough, they start interacting nonlinearly: the tearing instability saturates and an energy cascade to small scales is generated. At this stage of the time evolution, we consider the total energy spectrum $E^{\mathrm{tot}}_{m,n}(x,t)$ in the m-n plane, at a given position x. This is defined by

$$E^{\mathrm{tot}}_{m,n}(x,t)=\frac{1}{2}|\mathbf{B}_{m,n}(x,t)|^2+\frac{1}{2}|\mathbf{V}_{m,n}(x,t)|^2. \tag{18}$$

In positions x distant from the current sheet, the energy spectrum clearly develops in the direction perpendicular to the local equilibrium magnetic field. This can be seen in Fig. 3, where contour plots of $\log[E^{\mathrm{tot}}_{m,n}(x,t)]$ are shown at $x=-0.5$ and $t=35$. The dashed line indicates the local direction of $\mathbf{B}_0$ and it is perpendicular to the solid line, which is a good indication of the energy cascade direction. Then, in the region where $\mathbf{B}_0$ is relatively uniform, the spectral anisotropy corresponds to that of homogeneous MHD turbulence.

However, in a position close to the center of the current sheet, the spectral anisotropy is more complex and rapidly evolves in time. In Fig. 4, the energy spectrum at $x=-0.15$

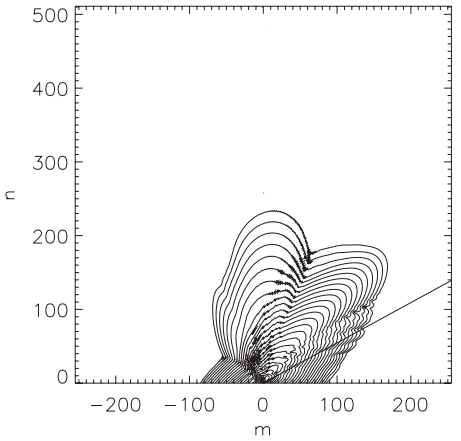

FIG. 4. Contour plots of the total energy spectrum $\log_{10}[E^{\mathrm{tot}}_{m,n}(x,t)]$ at $t=34$ and $x=-0.15$. The straight line is perpendicular to the equilibrium magnetic field.

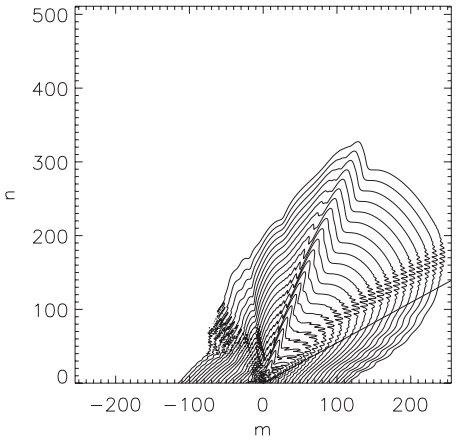

FIG. 5. The same as in Fig. 4, but at $t=35$.

and $t=34$ is plotted. Several lobes are present, even if two lobes are dominant: one lobe shows a tendency to be aligned along the direction locally perpendicular to $\mathbf{B}_0$ (indicated by a straight line), while the other lobe is approximately in the z direction. The latter lobe seems not to respect the rule that the cascade take place perpendicularly to $\mathbf{B}_0$. This behavior can be understood considering the properties of tearing-unstable modes. Each unstable mode is associated with a resonant surface, whose location is defined by the condition $mB_{0y}(x)+nB_{0z}(x)=0$. Thus, the wave vector (m,n) of the unstable mode is perpendicular to $\mathbf{B}_0(x)$ at the position where the corresponding resonant surface is located. The most unstable modes in this configuration have wave vectors with $m=0$ and a resonant surface at $x=0$ (Fig. 1). However, the energy of an unstable mode is not localized exactly on its resonant surface: unstable modes with resonant surface at $x=0$ present two peaks out of the current sheet. This is illustrated in Fig. 2, where the component $B_x(x)$ of magnetic-field perturbation of a linear unstable mode with $m=0$ is plotted. We see that, though the resonant surface of this mode is located at $x=0$, the energy of the perturbation is maximum at $x\pm 0.1$. Then, the lobe developed in the z direction at $x=-0.15$ (Fig. 4) can be interpreted as due to the $m=0$ modes, which are the most unstable, and whose energy is maximum around the position where the spectrum of Fig. 4 is calculated. In a similar way, the other minor lobes that are visible in Fig. 4 are due to other less unstable modes that have various wave vectors and resonant surfaces not located at the position where the spectrum is calculated.

At the same position $x=-0.15$, but at later times ($t=35$), the spectrum is dominated by a unique lobe, whose direction is nearly perpendicular to the local equilibrium magnetic field (Fig. 5). The lobe in the z direction due to the growth of unstable modes, which was present in the spectrum at previous times, tends to disappear with increasing time. Using the above linear code [18], we verified that the modes with resonant surface at this location ($x=-0.15$) are not linearly unstable (this is a consequence of periodicity that requires integer components for the wave vector), and that all the linearly unstable modes in this configuration have resonant surfaces at $|x|<0.1$. This is illustrated in Fig. 6, which represents the wave vectors (m,n) of all the unstable modes (m and n are integer numbers). For all these modes, the resonant surface is located at $|x|<0.1$, the position $|x|\simeq 0.1$ corresponding to the mode $(m,n)=(3,2)$. Therefore, the development of the lobe nearly perpendicular to $\mathbf{B}_0$ at $x=-0.15$ is not due to the growth of unstable modes, but to the nonlinear cascade in a more turbulent situation where the linear modes tend to disappear.

In Fig. 7, we show the time evolution of the x-integrated energy spectrum, defined by

$$e^{\mathrm{tot}}_{m,n}(t)=\int E^{\mathrm{tot}}_{m,n}(x,t)dx. \tag{19}$$

At time $t=32$, the spectrum is characterized by different lobes. This is a consequence of the superposition of different unstable modes with different resonant surfaces. Due to periodicity, the resonant surfaces of unstable modes are located at discrete positions determined by the ratio m/n, so there is a finite number of unstable modes and resonant surfaces are

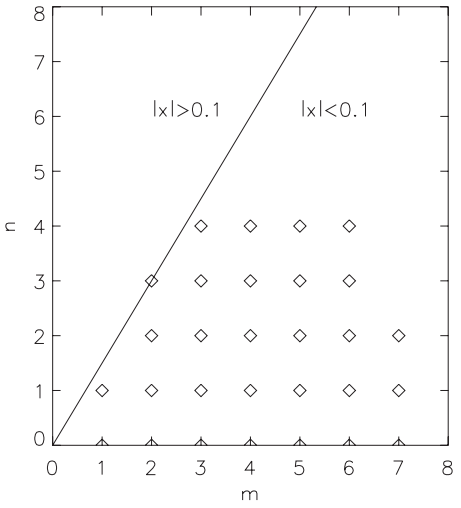

FIG. 6. All the unstable modes (indicated by diamonds) have resonant surfaces at $|x|<0.1$. The straight line corresponds to $m/n=1.5$, with a resonant surface at $x\simeq -0.097$. Only one unstable mode $(m/n=3/2)$ has a resonant surface at this location.

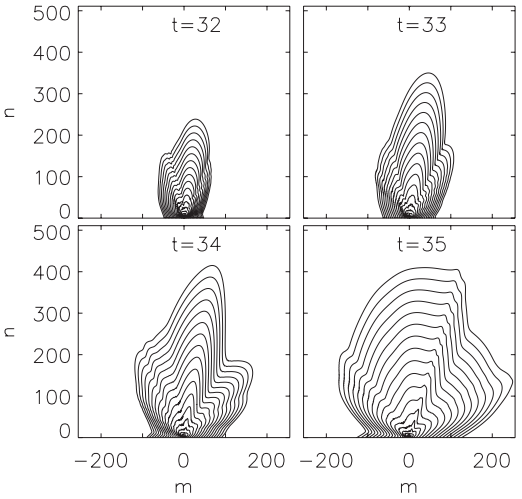

FIG. 7. Contour plots of the integrated energy spectrum $\log_{10}(e^{\mathrm{tot}}_{m,n})$ at different times.

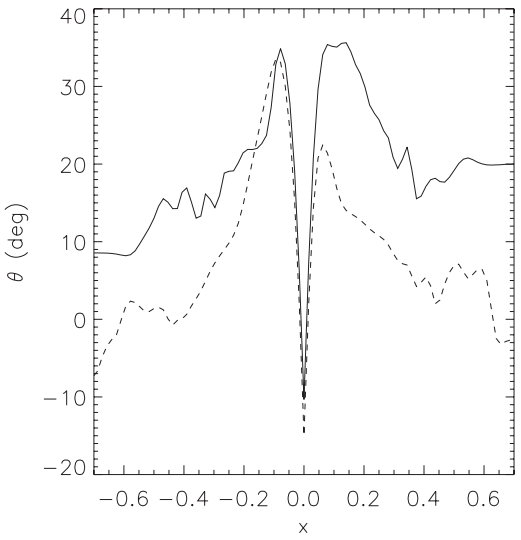

FIG. 8. The angle $\theta=(\alpha+|\alpha_B|)-90°$ at $t=34$ (solid line) and $t=35$ (dashed line).

distributed at discrete locations. With increasing time, the x-integrated spectrum tends to become more and more isotropic (Fig. 7), while the spectrum calculated at a fixed position x becomes increasingly anisotropic (Figs. 4 and 5). This can be understood considering that in the early phase of the time evolution, the spectrum anisotropy is determined mainly by the growth of the unstable modes, except very far from the center of the current sheet. As nonlinear effects become more important, the configuration becomes increasingly turbulent and the formation of the spectrum is affected by the direction of the energy cascade. Therefore, at each x location the energy spectrum (18) becomes more and more anisotropic. However, the preferred direction of nonlinear cascade [perpendicular to the local $\mathbf{B}_0(x)$] is different at different x positions and it covers a wide angle in the wave-vector plane varying with x. As a consequence, the x-integrated spectrum (19) becomes more isotropic, as shown in Fig. 7.

To give a measure of the local spectrum anisotropy, we calculated the anisotropy angle

$$\alpha(x) = \tan^{-1}\sqrt{\frac{\langle k_z^2(x)\rangle}{\langle k_y^2(x)\rangle}}, \tag{20}$$

where $\langle k_y^2(x)\rangle$ and $\langle k_z^2(x)\rangle$ are defined as

$$\langle k_z^2(x)\rangle = \frac{\sum_{m,n} n^2 E_{m,n}(x)}{\sum_{m,n} E_{m,n}(x)}, \tag{21}$$

$$\langle k_y^2(x)\rangle = \frac{\sum_{m,n} m^2 E_{m,n}(x)}{\sum_{m,n} E_{m,n}(x)}. \tag{22}$$

For an isotropic spectrum, the angle α would be 45°. We also define the angle $\theta(x)=[\alpha(x)+|\alpha_B(x)|]-90°$, where $\alpha_B=\tan^{-1}(B_{0z}/B_{0y})$ is the angle formed by the equilibrium magnetic field with the y axis. The angle $\theta(x)$ would be 0 if the energy cascade direction was perpendicular to the direction of the local equilibrium magnetic field. Figure 8 shows $\theta(x)$ at two different times. The angle $\theta(x)$ is closer to 0 far from the current sheet, where no unstable modes are present. A measure of the departure of $\theta(x)$ from 0 is given by the quantity

$$\delta\theta = \sqrt{\int_{-1}^{1} \theta^2(x)dx}. \tag{23}$$

We find $\delta\theta \simeq 25$ at $t=34$ and $\delta\theta \simeq 15$ at $t=35$. Then, $\theta(x)$ decreases everywhere in time. This is because unstable modes become less important and the consequences of the nonlinear energy cascade become more visible.

V. CONCLUSIONS

We studied the anisotropy of incompressible MHD turbulence generated by magnetic reconnection in a three-dimensional configuration with a sheared magnetic field. The formation of the turbulent spectrum is determined by nonlinear interactions which are more effective for wave vectors perpendicular to the local equilibrium magnetic field. The growth of the linearly unstable modes also has the effect of modifying the spectrum, but mainly in the early stage. The energy of the most unstable modes is localized around $x=\pm 0.1$ and it becomes visible in the spectrum at these locations with the presence of a lobe in the z direction. Later this contribution becomes less important: the configuration is increasingly more turbulent and less reminiscent of the initial instability. Then, the spectrum becomes dominated everywhere by wave vectors locally perpendicular to the direction of the equilibrium magnetic field. The x-integrated spectrum becomes increasingly isotropic, while at each x location the local spectrum becomes more and more anisotropic. The properties of anisotropy change in time, the growth of the

unstable modes becomes less important, and the energy cascade is dominated by wave vectors perpendicular to the equilibrium magnetic field. We suggest the possibility that these results could be used as a signature of nonlinear magnetic reconnection both in space and in laboratory plasmas and they can also help to identify the transport regime of energetic particles in a turbulent magnetic field, which is strongly influenced by the turbulence anisotropy [12,13].

[1] J. V. Shebalin, W. H. Matthaeus, and D. Montgomery, J. Plasma Phys. **29**, 525 (1983).
[2] T. S. Horbury, M. A. Forman, and S. Oughton, Plasma Phys. Controlled Fusion **47**, B703 (2005).
[3] Z. Vörös *et al.*, Ann. Geophys. **21**, 1955 (2003).
[4] S. J. Zweben, C. R. Menyuk, and R. J. Taylor, Phys. Rev. Lett. **42**, 1270 (1979).
[5] M. Onofri, P. Veltri, and F. Malara, Phys. Plasmas **14**, 062304 (2007).
[6] A. Retino, D. Sundkvist, A. Vaivads, A. Mozer, M. Andre, and C. J. Owen, Nat. Phys. **3**, 236 (2007).
[7] D. Sundkvist, A. Retino, A. Vaivads, and S. D. Bale, Phys. Rev. Lett. **99**, 025004 (2007).
[8] J. T. Gosling, R. M. Skoug, D. J. McComas, and C. W. Smith, J. Geophys. Res. **110**, A01107 (2005).
[9] J. T. Gosling, Astrophys. J. Lett. **671**, L73 (2007).
[10] T. D. Phan *et al.*, Nature **439**, 175 (2006).
[11] J. T. Gosling, S. Eriksson, T. D. Phan, D. E. Larson, R. M. Skoug, and D. J. McComas, Geophys. Res. Lett. **34**, L06102 (2007).
[12] G. Zimbardo, P. Pommois, and P. Veltri, Astrophys. J. Lett. **639**, L91 (2006).
[13] G. Qin, W. H. Matthaeus, and J. W. Bieber, Astrophys. J. Lett. **578**, L117 (2002).
[14] W. M. Elsässer, Phys. Rev. **79**, 183 (1950).
[15] S. Oughton, E. R. Priest, and W. H. Matthaeus, J. Fluid Mech. **280**, 95 (1994).
[16] J. Cho and E. T. Vishniac, Astrophys. J. **539**, 273 (2000).
[17] L. J. Milano, W. H. Matthaeus, and P. Dmitruk, Phys. Plasmas **8**, 2673 (2001).
[18] M. Onofri, L. Primavera, F. Malara, and P. Veltri, Phys. Plasmas **11**, 4837 (2004).